

# Optimal stimulation frequency for vibrational optical coherence elastography

Zhang, Duo; Wang, Jinjiang; Li, Chunhui; Huang, Zhihong

*Published in:*
Journal of Biophotonics

*DOI:*
10.1002/jbio.201960066

*Publication date:*
2020

*Document Version*
Peer reviewed version

# Optimal Stimulation Frequency for Vibrational Optical Coherence Elastography (OCE)

Duo Zhang[a], Jinjiang Wang[b], Chunhui Li[a,*], Zhihong Huang[a]

[a] School of Science and Engineering, University of Dundee, Dundee DD1 4HN, Scotland, UK;
[b] School of Precision Instruments and Optoelectronics Engineering, Tianjin University, Tianjin, P.R.China, 300072
[*]Corresponding Author: Dr Chunhui Li (c.li@dundee.ac.uk) +44(0)1382386730

**Abstract**: Vibrational optical coherence elastography (OCE) is a promising tool for extracting the mechanical property of soft tissue. Purpose of this study is focusing on settling the optimal frequency range for vibrational OCE with evenly distributed stress filed. A finite element model of 2% agar phantom was built by ANSYS with a vibration stimulation frequency range from 200 Hz to 3,000 Hz. Practical experiments were carried out for cross-validation with the same frequencies and sample. Lateral and horizontal stress filed distributions under different frequencies were mathematically evaluated by coefficient of variance and degree of linearity. Results from simulation and practical experiment cross-validated each other and 1,000 Hz was set as the maximum ideal frequency for vibrational OCE, while the minimum frequency is set by theoretical calculation with a result of 250 Hz. An ex-vivo biological sample was utilized to testify performance of vibrational OCE with excitation frequencies in and out of concluded optimal range, which showed that stiffness was better mapped out in optimal frequency range.

**Keywords:** vibration elastography; optical coherence elastography; mechanical property; optimal frequency

## 1. Introduction

Stiffness is one of the most important mechanical properties of human tissue, which is closely related to pathological conditions [1], it severs as a signature to distinguish benign and lesion tissue in clinics, for instance, prostate cancer [2] and breast cancer [3]. This functional imaging modality explores stiffness contrast is termed as elastography.

Elastography has been developed in medical imaging to aid diseases localisation, diagnosis and treatment monitoring. It is commonly based on imaging techniques, such as ultrasound based elastography [4] and magnetic resonance elastography [5], they

This article has been accepted for publication and undergone full peer review but has not been through the copyediting, typesetting, pagination and proofreading process which may lead to differences between this version and the Version of Record. Please cite this article as doi:10.1002/jbio.201960066

have been widely studied and applied for the diagnosis and evaluation of the treatment responses in many diseases, e.g. breast cancer [6], cardiology [7] and liver fibrosis staging [8]. But the resolution of ultrasound imaging and MRI systems are relatively low, that limits the application of early tumour detection with a size of 100 μm [9]. Optical coherence elastography (OCE) stands out with the inherited advantages from optical coherence tomography (OCT), with high resolution in micrometre scale [10] and high sensitivity above 90 dB [11]. OCT also offers high displacement sensitivity with the capability to detect deformation in nanometre scale, phase sensitive OCT (PhS-OCT) built by Wang *et al.* [13] could detect deformation in 10 nm, common path Fourier domain OCT established achieved a displacement sensitivity of 0.34 nm [12].

Among all the OCE technologies, vibrational OCE offers a higher resolution compared with wave based OCE [16]. Meanwhile, the algorithm for vibrational OCE employs fast Fourier transform (FFT) to resolve vibration amplitude only associated with excitation frequency, by which means noise and other co-generated vibration modes are eliminated, leading to an enhanced SNR [13].

Noted that mechanical property of sample cannot be detected directly, instead, mechanical loading measured by OCT system, vibration amplitude of periodic loading in axial direction, is going to be detected to infer relative stiffness. To enhance calculation efficiency, assumption has been proposed that stress is distributed uniaxially and uniformly, sample being analysed is isotopically elastic. Under this scenario, elasticity is inversely proportional to the amplitude strain, which is the depth derivative of deformation amplitude. As a result, guarantee of evenly distributed stress field is vital to retrieve reliable mechanical result.

There are several parameters that will affect stress distribution, including excitation frequency, amplitude of coupled excitation, geometry and size of feature. Several publications have illustrated those factors that impact stress distribution: Ponnekanti *et al.* [14] reported that stress concentration arises between feature boundaries, Kennedy *et al.* [15] demonstrated feature geometry has an impact on stress distribution. However, none of the publications mentioned impact induced by frequency that viscosity interferes the result when the frequency is too low, while for high stimulation frequencies, vibrational modes of sample are undesirable as concentrated stress filed will appear, leading to huge artefacts of the deformation profile. Frequency used for loading varies, leading to challenge of evaluating performance of different systems, and the results cannot be compared. At the moment, there is no consensus among research teams, Kennedy *et al.* [17] used 850 Hz as the driving frequency to reduce the effect of viscosity, Liang *et al.* [18] selected stimulation frequency varies from 20 Hz to 313 Hz, one year later, their team introduced compression load with a frequency range from 50 Hz to 250 Hz [19]. An optimal frequency range needs to be settled to guarantee an evenly distributed stress field.

To set an optimal frequency for vibrational OCE, we explored vibration results from

simulation and practice for 2% agar phantom. A finite element mode was constructed by harmonic response finite element model, compression loading at a frequency range from 200 Hz to 3,000 Hz are introduced to sample, axial deformation and strain distribution are generated and retrieved after simulation finished. Practical experiments were also implemented with the same conditions as simulation. Uniformity of stress filed are finally evaluated by deformation profile retrieved from both simulation and practical results. Quantitative evaluation was performed on the deformation profile in vertical and lateral direction by 2$^{nd}$ polynomial fitting and coefficient of variance respectively. Thresholds of frequency are determined to ensure uniformity of stress field by referring the quantitative evaluation, an optimal range from 250 Hz to 1,000 Hz is selected. Phantom and real biological sample of beef liver is tested in the end to validate the performance of vibrational OCE, with frequencies in and out of the optimal frequency range. The framework and results mentioned in this paper not only offers insight for vibrational OCE but also for other elastography imaging techniques that employ periodic loading.

# 2. Methods

## *2.1 Finite element simulation*

Harmonic response in ANSYS 14.5 is utilized to simulate vibration of sample with sinusoidal excitation in steady state. It accords with practical experiment where scanning begins after sample enters steady state. 2% agar, a commonly used material for tissue mimicking phantom with a homogeneous elasticity measured to be 193 kPa by our previous study [20], is selected to be the material. Its density is set to 1,000 kg/mm$^3$ with a passion ratio of 0.495 in finite element model.

Geometry is configured to be a cuboid with an equal edge length of 4 mm at base and a depth of 5 mm. Meshing size of the model is 0.125 mm to minimize the number of meshing nodes as well as computational time required by ANSYS. The meshing resolution covers all waves propagating inside sample with a speed of 1,500 m/s reported by Zell *et al*. [21], it is capable of delineating vibration inside sample.

An axial sinusoidal compression is applied on the bottom plane of sample with an amplitude identical to the performance of mechanical shaker used for practical experiment, expressed as black arrow in Figure 1 left. Top surface of sample is fixed where the fixed surface is rendered as blue. Friction is not considered at top and bottom surfaces; lateral expansion is allowed at all planes. The configuration simulates practical experiment which is illustrated in the next section. Frequency selected has an equal interval of 200 Hz from 200 Hz to 1,000 Hz, 500 Hz from 1,500 Hz to 3,000 Hz. The lower boundary of frequency range is selected by calculation, where viscous component takes less than 10% of the measured stiffness, illustration in detail is

discussed in appendix. Maximum frequency is selected from practice where concentrated stress filed is evidently observed.

Two paths, in lateral and vertical direction respectively, are selected from the mid cross-section plane to retrieve deformation data, as shown in Figure 1 right. Data collected will be analysed and quantified to evaluate performance of OCE at certain frequencies. Methods are illustrated in the following sections.

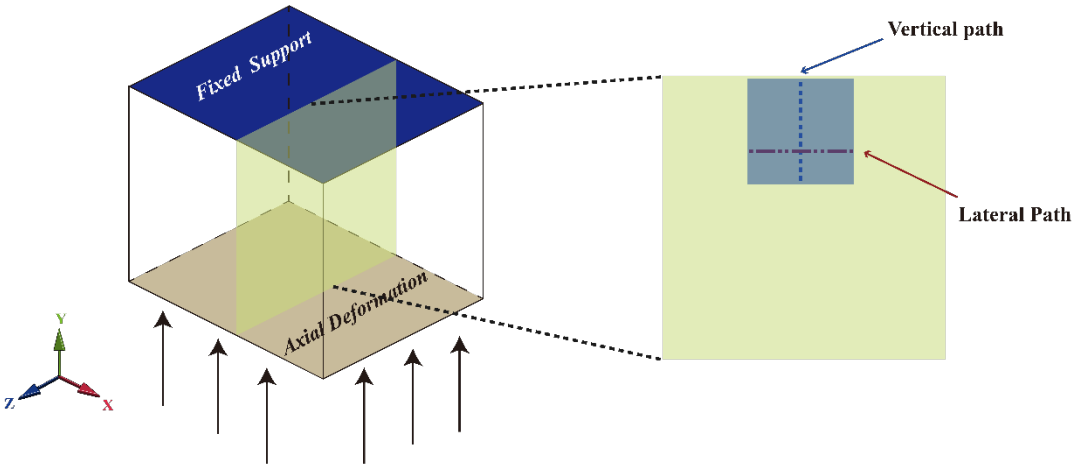


Figure 1 ANSYS simulation. Left: The top surface in blue indicates the fixed support. Black arrow to the bottom represents axial deformation applied to the bottom surface. Right: Dashed lines to the right imply the two paths for analysis of strain distribution in both lateral and axial direction.

## *2.2 Practical Experiment*

**Phantom**

Two percent agar phantom, the same material for simulation, is fabricated with 2 g agar powder solved in 100 g distilled water, after which the solvent is stirred for 1 h and poured into the mode to cure.

One percent titanium dioxide ($TiO_2$) solvent is added as scattering by mixing distilled water and $TiO_2$ powder. Mechanical stir of 10 minutes is applied to diminish and minimize size of the clusters. The $TiO_2$ solution concentration added to phantoms are 0.6 mg/ml. Our compressional test of phantoms added with $TiO_2$ scatterings has proven that the addition of $TiO_2$ scattering will not alter elasticity of phantoms.

**Ex-vivo biological sample**

Beef liver (fresh, bought from local butcher) is utilized as real biological sample for practical experiment to test performance of vibrational OCE at several frequencies. Stiffness contrast on beef liver is achieved by using high intensity focus ultrasound (Transducer G701#, Chongqing Haifu Medical Technology Co., Ltd, China) that impinging high energy upon certain area of tissue for 10s with a frequency of 10 MHz, specifications are attached in our previous publication [22]. Area been treated, referred

as lesion, possesses a larger stiffness respect to the surrounding normal tissue due to damage of original structure and the constituent material from heat [23]. One percent agar phantom is employed as a standard reference with known stiffness around 80 kPa [20], beef liver is embedded inside agar phantom such that coupling between glass window and surface of sample is uniform. Stiffness contrast between 1% agar and treated beef liver is also large enough to generate an evident difference in elastogram.

Excitation of sinusoidal deformation with 850 Hz and 1,500 Hz is applied to sample, whose amplitude is similar such that strain measured is in the same level and comparison can be achieved. The two frequencies selected is intentioned that 850 Hz is in the optimal frequency range while 1,500 Hz is out of the range.

**System Setup**

A practical vibrational OCE experiment has been designed to cross-validate results from ANSYS simulation. Our group at University of Dundee assembled phase sensitive common path OCT (PhS-OCT) as well as a vibrator to construct vibrational OCE, configuration is shown in Figure 2. Super-luminescent laser diode (Thorlabs LS2000B) is employed as light source with a central wavelength of 1,340 nm with full width at half maximum (FWHM) of 110 nm, comprising an axial resolution of 7 μm in theory and 7.8 μm in practice. Focal length of objective lens is 50 mm, denoting a theoretical lateral resolution of 16 μm. The OCT system is configured as common path mode where the original reference arm is shaded and the lower surface of imaging window (Ø1" N-BK7 Broadband Precision Window, Uncoated, t = 5 m, Thorlabs), denoted as window in Figure 2, serves as reference plane whose reflection shares the same path with sample arm. This configuration greatly increases sensitivity of the setup [24], with a sensitivity of 50 dB measured at an exposure time of 6.96 μs. The displacement sensitivity for PhS-OCT is tested to be 2 nm with a static reflection mirror, corresponding signal to noise ratio is 53 dB. The high-speed InGaAs line scan camera (SUI, Goodrich Corp, NJ, USA) with 1,024 pixels coupled with a transmission grating (1,200 lines/mm) and lens, comprises an interferometer to detect and collect interfered signal, whose maximum sampling frequency reaches 91,912 kHz.

Window is located 1-2 mm above focus of objective lens and fixed, sample is placed in between vibrator and glass window. Compression load induced from vibrator has a sinusoid pattern with an amplitude proportional to the given voltage. To ensure direct and uniform contact between sample and window, a bulk static compression is induced, after which a sinusoidal compression load is coupled on the bottom surface of sample. Data collection begins after sample reaches its steady state and scan is acquired at a speed of 20,730 A-lines/s. Lateral scanning range depends on the scanning angle of galvanometer which is controlled by the hardware and fully programmable.

To obtain 2D cross-sectional deformation profile, MB-scan is applied with 512 A-scans for one M-scan and 512 M-scans allocated on the 1.67mm line are incorporated in the

end. Local axial deformation of each pixel is calculated by FFT of phase difference of 512 A-scans, local strain is obtained from vertical slop of deformation by continuous wavelet transform of Gaussian1 wavelet [25]. Frequency is selected to be the same with simulation with a range 200 Hz to 3,000 Hz.

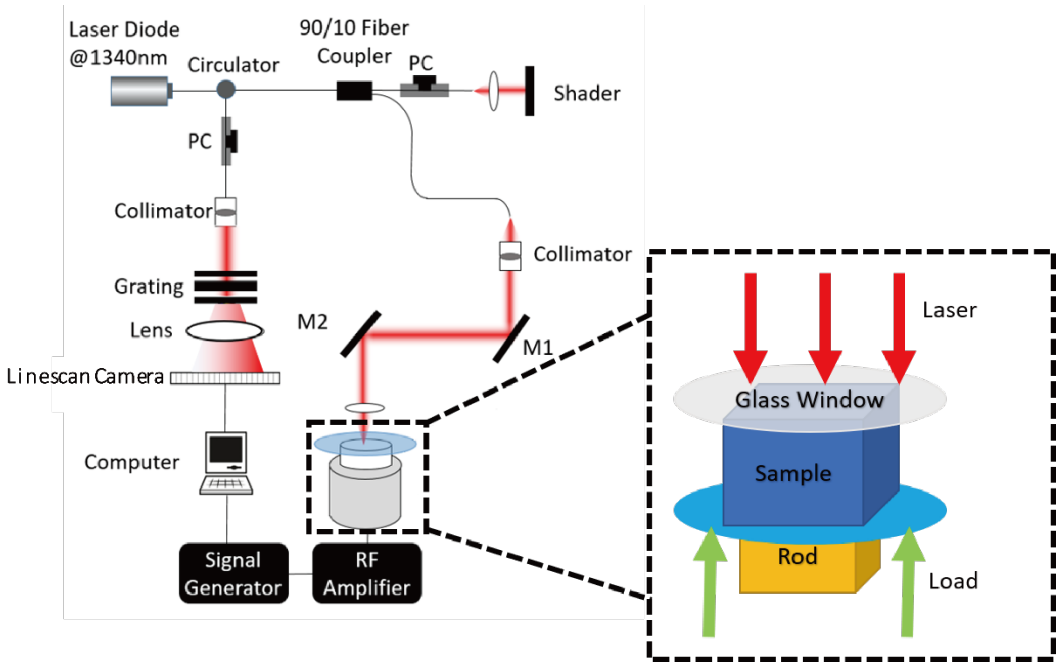


Figure 2 Vibrational OCE setup, composed of two major parts of phase sensitive OCT and vibration stimulation. M1 & M2 Galvanometers mirrors, PC polarization controller. The vibration stimulation assembly is enlarged to illustrate in detail shown in the right, sample is placed in between fixed glass window and vibration plate attached to rod of vibrator. Sinusoidal loading is administrated from bottom by vibrator. Direction of loading is shown in green arrow, points upwards in axial direction which is parallel to laser.

**Quantitative Evaluation of Stress Field Distribution**

Uniformity of stress field is measured by distribution of strain, as 2% agar phantom is isotopically elastic, ratio between strain and stress is expected to be a constant. Second order polynomial fitting is administrated to deformation in vertical direction to depict relationship between deformation amplitude and depth, the absolute ratio between coefficient of the 1st order term as well as the 2nd order term illustrates the degree of linearity [26], which represents uniformity of strain.

$$Amp = Ad^2 + Bd + C \quad (1)$$

$$R = abs(B/A) \quad (2)$$

The 1st order term, $A$ in Equ.1, represents linear component and the 2nd term $B$ stands for the nonlinear, quotient between the two shown in Equ.2 implies a comparison. Dominant linear component will result in a large value of the ratio, vice versa. The constant term $C$ is not taken into consideration for the analysis.

To quantify dispersion of stress field along lateral direction, coefficient of variation (CV) is administrated to deformation data on a lateral path, as uniformity of strain in one lateral path is reflected by deformation contour: a laterally flat contour indicates a uniform strain field. CV is defined as ratio between standard deviation and the mean, it is a standard measurement of dispersion. An evenly distributed stress filed along lateral direction expects a flat contour with a low CV.

# 3. Results

## *3.1 Deformation Profile & Performance Evaluation*

Figure 4 and Figure 3 are axial deformation distribution on cross section plane for experiment and simulation respectively. Axial direction is defined to point upwards parallel to the paper, and deformation amplitude mentioned in the following sections are all in axial direction to accord with the fact that OCT is only able to detect deformation in axial direction. Colormaps to the right indicates the amplitude of vibration at excitation frequency in Fourier domain. Figure 4a to Figure 4h shows deformation profile with an increasing stimulation frequency from 200 Hz to 3,000 Hz, where an emerging stress concentration is observed by the curved-shape contour. Evident stress concentration is firstly revealed at 1,500 Hz that deformation contour is no longer laterally flat, three ellipse-shape contours at 3,000 Hz profile representing severer stress concentration.

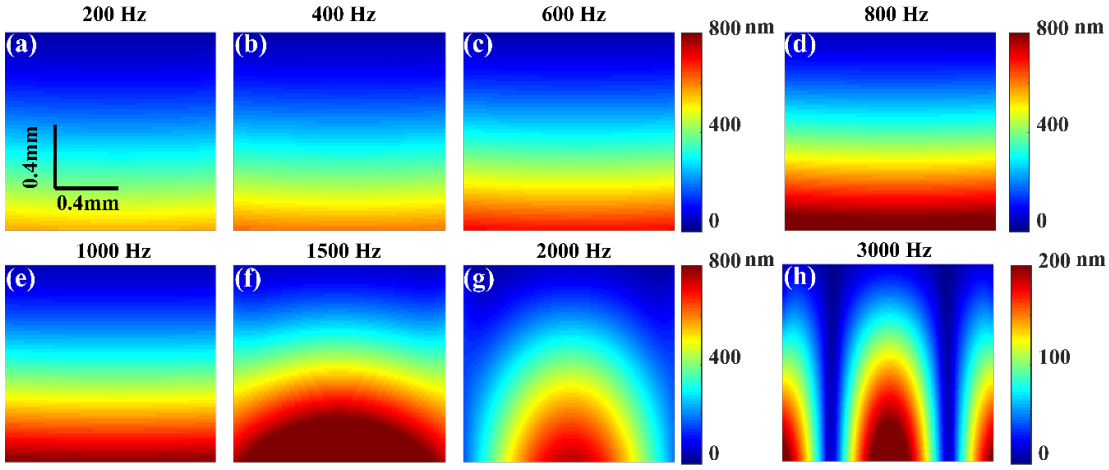


Figure 3 Amplitude of axial deformation on middle cross section plane for simulation, shown in **Error! Reference source not found.**, from a) to g) frequencies gradually increase from 200 Hz t o 3,000 Hz (a.200 Hz, b.400 Hz, c.600 Hz, d.800 Hz, e.1,000 Hz, f.1,500 Hz, g.2,000 Hz, h.3,000 Hz).

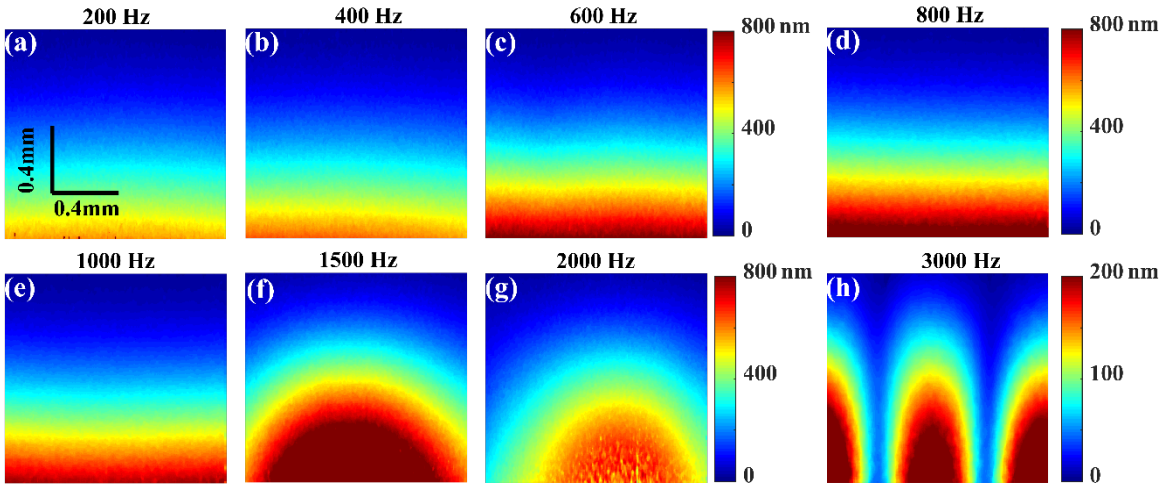


Figure 4 2D deformation profile for 2% agar phantom in practical experiment, frequency varies from 200 Hz to 3000 Hz. (a.200 Hz, b.400 Hz, c.600 Hz, d.800 Hz, e.1,000 Hz, f.1,500 Hz, g.2,000 Hz, h.3,000 Hz).

Coefficient of variation along lateral path is utilized to quantify stress distribution as mentioned above, whose result is shown in Figure 5 left where simulation data is rendered as blue solid line with green asterisks data points, experimental data is rendered as red dashed line with black dotted data points. Errors are too small when compared with CV that error bars are not included in the figure. Data values of simulation and experiment along frequency range are close to each other. The discrepancy, majorly located within 1,000 Hz, ascribes to the inevitable noise in practice, which adds dispersion of deformation. A rapid CV growth is observed beyond 1,000 Hz and reaches a value larger than 0.4, representing a development of stress concentration. It accords to the 2D profile revealed by Figure 3 and Figure 4 that contour appears after 1,000 Hz, and the curvature increases respect to frequency.

Quantitative evaluation of stress field in vertical direction is applied to deformation to depth data that is located on the vertical path, shown in Figure 1. The algorithm for evaluation is introduced in last section expressed in Equ.2.
Figure 5 right shows the ratio between 1$^{st}$ order term and the 2$^{nd}$ order term of polynomial fitting on vertical deformation profile within 1,000 Hz. The upper border of analysed frequency is selected by CV value shown in Figure 5 left that lateral uniformity of stress field is ensured. Experimental data with error bars is plotted in blue solid line, its corresponding data points are illustrated as blue dots. Simulation data is rendered in dashed purple line with asterisk data points. The overall R value varies slightly, implying the low correlation between excitation frequency and stress distribution along vertical direction in the limited field of view. The relatively huge error bar lies in the noise and fitting algorithm that incorporates error points in 2$^{nd}$ fitting facilitating erroneous fitted line.

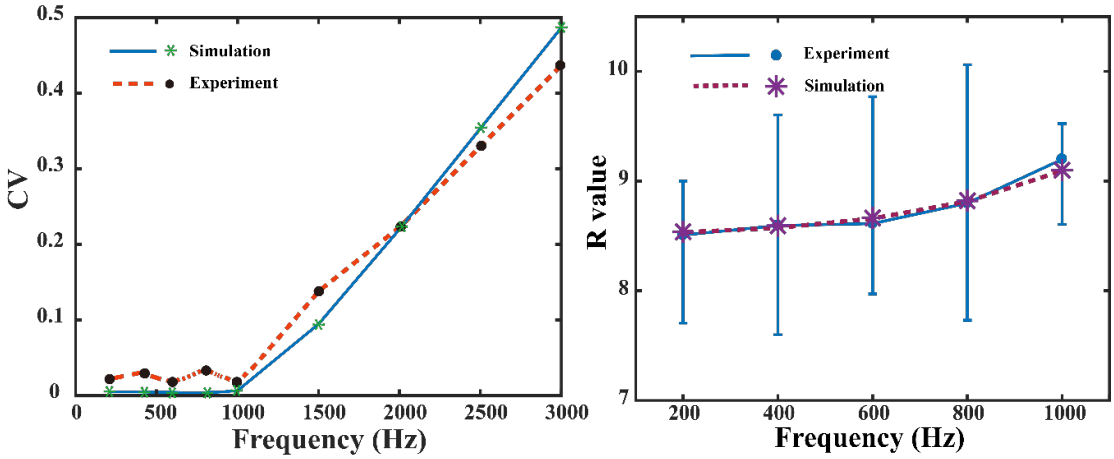


Figure 5 Left: Coefficient of variation (CV) at lateral path. The path been analysed is shown in **Error! Reference source not found.** as the brown dashed line. Simulation data is rendered as blue solid line with green asterisk data points. Experimental data is plotted as dashed red line with black dotted data points. Right: Ratio of 1st order term and the 2nd order term after 2nd order polynomial fitting of deformation profile. Experimental data is rendered as blue solid line with error bar, simulation data is plotted as dashed purple line with data points shown as asterisks.

## *3.2 Ex-vivo biological sample evaluation*

Structure image of ex-vivo biological sample is shown in Figure 6a that liver has a higher brightness located to the bottom and 1% agar is above the liver. Figure 6b and Figure 6c present 2D strain distribution where lesion area has a darker colour with a smaller strain, indicating a relative higher elasticity than the surrounding material. Green dashed line delineates the lesion area, denoted as region 4, where a close geometrical correspondence is revealed that lesion area shown in strain map accords with structure image. Region 3 highlights liver tissue without treatment, contrast between untreated and treated tissue decreases as frequency reaches beyond optimal frequency range. Average strain is calculated on the central areas of 4 regions to avoid stress concentration near the boundary, while strain contrast is defined as the ratio between average strain. Result is shown in Table 1, where strain contrast between 1% agar phantom at region 1 and region 2 increases from 1.27 to 1.66, and contrast between untreated and treated beef liver drops from 2.30 to 2.03. Strain ratio between treated liver and 1% agar located to the above (Region 1) increase slightly, correlating to the stress distribution in vertical direction curve (Figure 5 right) that the R value increases slowly respect to frequency. Estimated stiffness of treated beef liver is 199.2 kPa with an average strain ratio of 2.49 between region 1 and region 4 and known 1% agar stiffness of 80 kPa.

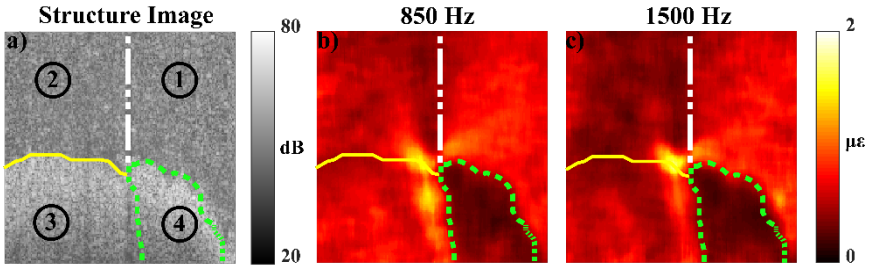


Figure 6 Strain mapping of biological sample. a) Structure image in dB scale, where beef liver is located to the bottom. b),c) strain distribution along the 2D plane, where colour bar attached represents the strain is in micro-scale. Four areas are separated to prove impact of frequency that imposed on stress distribution. Region1 and region 2 are 1% agar phantom; Beef liver without treated is in region 3; Section depicted by green dashed line, region 4, highlights section of beef liver treated by high intensity focus ultrasound.

**Table 1 Strain contrast.**

| Region \ Frequency | 850 Hz | 1,500 Hz |
|---|---|---|
| **Region 1 / Region 2** | 1.27 | 1.66 |
| **Region 3 / Region 4** | 2.30 | 2.03 |
| **Region 1/ Region4** | 2.45 | 2.54 |

# 4. Discussion

This paper demonstrates optimal frequency for vibrational OCE, which confirmed by a cross-validation between finite element model and practical experiment. As local stress is impossible to measure inside sample, assumptions has been proposed that stress is uniform and uniaxial such that stiffness contrast is deduced from strain. Under this scenario, guarantee of a uniformly distributed stress is vital to perform vibrational OCE. This study proves limitations imposed by excitation frequency with statistical analysis that stress concentration appears with an excitation frequency above 1,000 Hz, thus a maximum excitation frequency is set. This study is promising and can offer guidance for future research, as framework presented in this paper can also be extended and adapted for other imaging based elastography modalities which incorporate periodic loading.

Two dimensional deformation distribution on the cross-section plane is displayed in Figure 3 and Figure 4 for simulation and experiment respectively. The correspondence between the two shows that excitation frequency has an impact on stress filed distribution that higher frequency is more possible to generate concentrated stress filed. Rapid growth of CV value after 1,000 Hz implies appearance and development of stress concentration. Reason may lie in modal superposition where several vibration modes overlay to form crest and trough in a short distance, representing by laterally anisotropic deformation profile, as shown in Figure 4g, but the hypothesis still needs to be proved and validated in the future. No matter what mechanical basis stress concentration

ascribes to, it is rational to propose that stress concentration is more possible to be detected with a driving frequency above 1,000 Hz than the frequency range below it. To avoid unevenly distributed stress field, an upper limit of frequency is set to 1,000 Hz in this study.

Quantitative evaluation of linearity along vertical direction, shown in Figure 5 right, proves that in the field of view for vibrational OCE, stress distribution in vertical direction has a low dependence on frequency in the analysed frequency range. R value below 1,000 Hz are all above 8 implying that linear component of $2^{nd}$ polynomial fitting is at least 8 times larger than nonlinear component. It represents a uniform strain distribution along the vertical direction, as stress is inversely proportional to strain in homogeneous material with isotropic elasticity, stress is also uniformly distributed. This conclusion is against intuition that stress concentration is going to appear in both directions, where linearity shown in Figure 5 should decrease. There are two explanations for the observing. First, limited by depth of view of OCT, analysis range is too small to reveal overall linearity of stress field distributed at cross-section plane. If depth range of simulation results is enlarged to show, an enclose contour will gradually come to shape as frequency increases where linearity or stress concentration in vertical direction is easily observed. Second, frequency range selected for stress distribution in vertical direction is dedicated by result from lateral direction, where 1,000 Hz is set as the upper limit. If the frequency is extended to 3,000 Hz or even higher, stress concentration in vertical direction can be observed.

With analysis mentioned above, stress distribution along both lateral and vertical direction can be avoided with an excitation frequency in 1,000 Hz. The uniformity of stress field supports previous assumption suggested by Kennedy *et al.* [28] that stress is uniform and uniaxial inside sample. However, for vibrational OCE in clinical use, other than frequency alone, factors, e.g. feature geometry and size, also imposes a deviation to ideal stress field. Kennedy *et al.* [29] has shown that sample size and stiffness contrast alter distribution of stress field. Figure 6 also shows that concentrated strain, direct reflection of stress concentration, appears at the boundary between lesion and agar phantom regardless of excitation frequency, this artefact is inevitable as complications of boundary conditions. Strain difference between 1% agar located in region 1 and region 2 implies a stress field variance at the corner of feature. Although further investigations are required to understand all the factors that determines stress field distribution, a proper frequency range still needs to be settled to ensure a relative uniform stress field. Strain contrast of biological sample, shown in Table 1, shows that the strain contrast between 1% agar phantom located in region 1 and region 2 respectively enlarges as frequency increases. The contrast boost between 1% agar phantom demonstrates stress uniformity loss as agar is an isotopically elastic material which means that a contrast of 1 is expected for best performance. While for contrast between treated and untreated beef liver, a larger contrast indicates a better performance of vibrational OCE. Contrast between these two regions (Region 1 and Region 4) drops from 2.30 at 850 Hz to 2.03 at 1,500 Hz, representing a contrast loss due to frequency.

Thus, results of strain contrast revealed by biological sample proves that an optimal frequency range must be settled to ensure the generated strain mapping is reliable to reveal stiffness distribution.

Lower boundary of excitation should also be set as vibration at low frequencies suffers from viscous effect which causes sensitivity loss of resulted elastogram. Theoretical derivation is attached in appendix to prove that mechanical contrast revealed by strain is predicted to become lower than expected when viscosity is not neglectable. To avoid evident viscous effect, a frequency of 250 Hz is selected as threshold. See appendix for detail information.

By combining finite element analysis and practical experiment, the optimal frequency for vibrational OCE is below 1,000 Hz, a theoretical calculation of the minimum frequency is 250 Hz, but further experiments are required to validate the impact of viscosity. Besides that, sample used for experiment in this paper is 2% agar phantom, frequency range derived from simulation and practice is only suitable for materials with similar mechanical property, e.g. soft tissue with an elasticity range from 50 kPa to 20 kPa. In clinical applications to measure the stiffness of in-vivo or ex-vivo, a proper frequency range may vary from this paper's conclusion as the optimal frequency range is dictated mainly by elasticity and viscosity of material, further evaluation is required to set an optimal frequency for certain applications. This paper only illustrates one of the impacts, stress field distribution brought by excitation frequency, which alters the accuracy of detected elastogram. Other impacts, such as true mechanical contrast in an anisotropic sample, are not evaluated. Our next paper will focus on the effect and basis of viscosity with low frequency excitation, to validate the lower boundary of optimal frequency range and to explore methods to quantify viscosity.

## 5. Conclusion

This paper proposes a term as the optimal frequency and a framework to settle the frequency for vibrational OCE, where an optimal frequency range is from 250 Hz to 1,000 Hz. Methodology used in this paper may also be adapted and extended to other elastography imaging techniques which incorporate periodic loading.

## Reference


1. V. Swaminathan, K. Mythreye, E. T. O'Brien, A. Berchuck, G. C. Blobe, R. Superfine Cancer Res. 2011, 71, 5075-5080.
2. S. E. Cross, Y.-S. Jin, J. Rao, J. K. Gimzewski Nature Nanotechnology. 2007, 2, 780.
3. V. Gkretsi, T. Stylianopoulos Frontiers in oncology. 2018, 8, 145.
4. R. M. S. Sigrist, J. Liau, A. E. Kaffas, M. C. Chammas, J. K. Willmann Theranostics. 2017, 7, 1303-1329.
5. Y. K. Mariappan, K. J. Glaser, R. L. Ehman Clinical anatomy (New York, N.Y.). 2010, 23, 497-511.
6. E. V. Gubarkova, A. A. Sovetsky, V. Y. Zaitsev, A. L. Matveyev, D. A. Vorontsov, M. A. Sirotkina, L. A. Matveev, A. A. Plekhanov, N. P. Pavlova, S. S. Kuznetsov, A. Y. Vorontsov, E. V. Zagaynova, N. D. Gladkova Biomedical optics express. 2019, 10, 2244-2263.
7. M. Strachinaru, J. G. Bosch, B. M. van Dalen, L. van Gils, A. F. W. van der Steen, N. de Jong, M. L. Geleijnse, H. J. Vos Ultrasound in medicine & biology. 2017, 43, 1596-1606.
8. R. G. Barr, G. Ferraioli, M. L. Palmeri, Z. D. Goodman, G. Garcia-Tsao, J. Rubin, B. Garra, R. P. Myers, S. R. Wilson, D. Rubens, D. Levine Radiology. 2015, 276, 845-861.
9. Esserman LJ and Joe BN. Clinical features, diagnosis, and staging of newly diagnosed breast cancer. In: UpToDate. Hayes DF, Burstein H, Vora SR (eds.). Waltham, MA: UpToDate, 2018.
10. M. Adhi, J. S. Duker Current opinion in ophthalmology. 2013, 24, 213-221.
11. A. Agrawal, T. J. Pfefer, P. D. Woolliams, P. H. Tomlins, G. Nehmetallah Biomedical optics express. 2017, 8, 902-917.
12. B. F. Kennedy, R. A. McLaughlin, K. M. Kennedy, L. Chin, A. Curatolo, A. Tien, B. Latham, C. M. Saunders, D. D. Sampson Biomedical optics express. 2014, 5, 2113-2124.
13. R. K. Wang, L. An Opt. Express. 2009, 17, 8926-8940.
14. H. Ponnekanti et al., "Fundamental mechanical limitations on the visualization of elasticity contrast in elastography," Ultrasound Med. Biol.21(4), 533–543 (1995).
15. K. M. Kennedy, C. Ford, B. F. Kennedy, M. B. Bush, and D. D. Sampson, "Analysis of mechanical contrast in optical coherence elastography," J. Biomed. Opt. 18(12), 121508 (2013).
16. F. Zvietcovich, J. Yao, Y.-J. L. Chu, P. Meemon, J. P. Rolland, K. J. Parker in A comparative study of shear wave speed estimation techniques in optical coherence elastography applications, Vol. (Ed.^Eds.: Editor), City, 2016.
17. B. F. Kennedy, T. R. Hillman, R. A. McLaughlin, B. C. Quirk, D. D. Sampson Opt. Express. 2009, 17, 21762-21772.
18. X. Liang, S. G. Adie, R. John, S. A. Boppart Opt Express. 2010, 18, 14183-14190.
19. B. F. Kennedy, X. Liang, S. G. Adie, D. K. Gerstmann, B. C. Quirk, S. A. Boppart,

D. D. Sampson Opt. Express. 2011, 19, 6623-6634.
20. C. Li, G. Guan, R. Reif, Z. Huang, R. K. Wang Journal of the Royal Society, Interface. 2012, 9, 831-841.
21. K. Zell, J. I. Sperl, M. W. Vogel, R. Niessner, C. Haisch Physics in medicine and biology. 2007, 52, N475-484.
22. Wang, G., Wang, Y., Zhou, K., Feng, K., Li, F., Li, C., & Huang, Z. (2018). High Intensity Focused Ultrasound (HIFU) Combines Optical Coherence Tomography(OCT) for Biological Tissue Treatment and Evaluation. In *2018 IEEE International Ultrasonics Symposium, IUS 2018* (Vol. 2018-October).
23. J. Vappou, P. Bour, F. Marquet, V. Ozenne, B. Quesson *Physics in Medicine & Biology*. **2018**, *63*, 095018.
24. A. B. Vakhtin, D. J. Kane, W. R. Wood, K. A. Peterson Appl. Opt. 2003, 42, 6953-6958.
25. L. Nie, S. Wu, X. Lin, L. Zheng, L. Rui Journal of Chemical Information and Computer Sciences. 2002, 42, 274-283.
26. Ch. 8 in Keith, T. Z. (2005). Multiple regression and beyond. Allyn & Bacon. 978-0205326440
27. Meyers and Chawla (1999): "Mechanical Behavior of Materials," 98-103.
28. B. F. Kennedy, K. M. Kennedy, and D. D. Sampson, "A review of optical coherence elastography: fundamentals, techniques and prospects," IEEE J. Sel. Top. Quantum Electron. 20(2), 272–288 (2014).
29. K. M. Kennedy, C. Ford, B. F. Kennedy, M. B. Bush, and D. D. Sampson, "Analysis of mechanical contrast in optical coherence elastography," J. Biomed. Opt. 18(12), 121508 (2013).
30. Y. Kuwahara, Y. Shima, D. Shirayama, M. Kawai, K. Hagihara, T. Hirano, J. Arimitsu, A. Ogata, T. Tanaka, I. Kawase; Quantification of hardness, elasticity and viscosity of the skin of patients with systemic sclerosis using a novel sensing device (Vesmeter): a proposal for a new outcome measurement procedure, Rheumatology, Volume 47, Issue 7, 1 July 2008, Pages 1018–1024

# Appendix

Property of viscoelastic material under vibratory state is express as dynamic modulus which equals to ratio of strain and stress [27]:

$$E' = \frac{\sigma_0}{\varepsilon_0}\cos(\delta) \qquad (Appendix-1)$$

$$E'' = \frac{\sigma_0}{\varepsilon_0}\sin(\delta) \qquad (Appendix-2)$$

Where $E'$ is storage modulus contributing to store energy and $E''$ is loss modulus resulting in energy dissipation. Strain and stress are defined as:

$$\sigma = \sigma_0 \sin(\omega t + \delta) \qquad (Appendix-3)$$

$$\varepsilon = \varepsilon_0 \sin(\omega t) \qquad (Appendix-4)$$

$\delta$ is phase lag between strain and stress, $\sigma_0$ and $\varepsilon_0$ are the amplitudes of stress and strain, $\omega$ is angular frequency of the vibratory state. The overall dynamic modulus is defined as:

$$E = E' + iE'' \qquad (Appendix-5)$$

To better investigate relationships among dynamic modulus viscosity and elasticity, Maxwell model is incorporated as:

$$E' = \frac{E}{1 + \frac{E^2}{\eta^2\omega^2}} \qquad (Appendix-6)$$

$$E'' = \frac{\eta\omega}{\frac{\omega^2\eta^2}{E^2} + 1} \qquad (Appendix-7)$$

$E$ and $\eta$ are elastic and viscous coefficients of material respectively. As OCT is only able to detect axial deformation respect to depth, strain can be acquired by mathematical derivative. From Equ.Appendix-6 and Equ.Appendix-7:

$$E'^2 + E''^2 = \frac{\sigma_0^2}{\varepsilon_0^2} \qquad (Appendix-8)$$

$$\varepsilon_0^2 = \sigma_0^2/(E'^2 + E''^2) \qquad (Appendix-9)$$

Stress is considered uniaxial and uniform under assumption mentioned in introduction part, thus for a sample anisotropic elasticity:

$$\varepsilon_0^2 \propto (E'^2 + E''^2)^{-1} \qquad (Appendix-10)$$

$$\frac{\varepsilon_a^2}{\varepsilon_b^2} = \frac{E_b'^2 + E_b''^2}{E_a'^2 + E_a''^2} \qquad (Appendix-11)$$

Strain contrast lies in the value $E'^2 + E''^2$ which can be linked with elasticity and viscosity by Maxwell model:

$$\varepsilon^{-1} \propto (E'^2 + E''^2)^{\frac{1}{2}} = \frac{\eta}{\sqrt{\eta^2 + \frac{E^2}{\omega^2}}} * E = \frac{1}{\sqrt{1 + \frac{1}{\omega^2\tau^2}}} * E = C * E (Appendix - 12)$$

$\tau$ is relaxation time constant $\tau = \frac{\eta}{E}$, $C = \frac{1}{\sqrt{1+\frac{1}{\omega^2\tau^2}}}$. Strain is inversely proportional to $C * E$, where C is a coefficient related to material viscoelasticity and vibratory frequency which is usually less than one. To maximize strain contrast, C is the larger the better. To relationship between axial deformation data collected by OCT and quantities that used to reveal stiffness contrast is represented as:

$$\varepsilon = \frac{\Delta d}{d} = \frac{d_1 - d_2}{\Delta Z} \qquad (Appendix - 13)$$

Where $d$ represents axial deformation amplitude, $Z$ is depth. Stiffness contrast internal sample is detected by strain variation, which equals to the slope difference of deformation amplitude respect to depth.

To set a lower limit for acceptable strain that is able to reveal elasticity accurately, mathematical calculation is applied to viscoelasticity expressed in Equ.Appendix-12. According to a relaxation test of 5% strain carried out by Kuwahara *et al.* [30], relaxation time of skin is around 1.5 ms, as 2% agar phantom is thought to have a similar property as skin, this value is utilized to estimate C in Equ.Appendix-12. Result is shown in Figure Appendix-1 where the C value increases as frequency rises, a value of 1 implies the 100% accurate and 0 indicates the opposite. To guarantee accuracy, threshold of C value is set to be 0.9, implying viscous influence is under 10 %, which accords to 250 Hz in figure, thus lower boundary of frequency range for stimulation is set as 250 Hz.

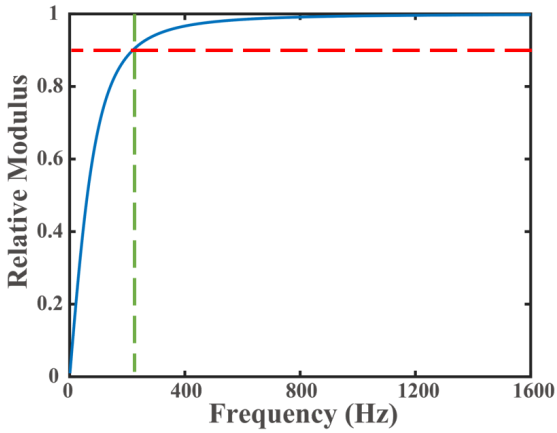


Figure Appendix-1 Relative Modulus with frequency of human skin. Relative modulus is defined as 1 to completely identical with elastic modulus, vice versa. The curve undergoes a monotonous rise, a value of 0.9 for relative modulus is set as threshold with corresponding frequency around 250 Hz.